Marine Pollution Bulletin 202 (2024) 116379

Contents lists available at ScienceDirect

Marine Pollution Bulletin

journal homepage: www.elsevier.com/locate/marpolbul

Comparing pre-industrial and modern ocean noise levels in the Santa Barbara Channel

Vanessa M. ZoBell *, John A. Hildebrand, Kaitlin E. Frasier

Scripps Institution of Oceanography, University of California San Diego, La Jolla, CA, USA

ARTICLE INFO

Keywords:
Ocean noise
Noise pollution
Shipping
Propagation
Modeling
Acoustics

ABSTRACT

To understand the extent of anthropogenic noise in the ocean, it is essential to compare the differences between modern noise environments and their pre-industrial equivalents. The Santa Barbara Channel, off the coast of Southern California, is a corridor for the transportation of goods to and from the busiest shipping ports in the Western hemisphere. Commercial ships introduce high levels of underwater noise into the marine environment. To quantify the extent of noise in the region, we modeled pre-industrial ocean noise levels, driven by wind, and modern ocean noise levels, resulting from the presence of both ships and wind. By comparing pre-industrial and modern underwater noise levels, the low-frequency (50 Hz) acoustic environment was found to be degraded by more than 15 dB. These results can be used to identify regions for noise reduction efforts, as well as to model scenarios to identify those with the greatest potential to support marine conservation efforts.

1. Introduction

Commercial shipping is the primary source of anthropogenic noise in the ocean, resulting in modern (post-industrial) ocean noise levels that have increased over the past few decades due to growth in the numbers and sizes of the vessels (Ross, 1976; Hildebrand, 2009; Wenz, 1962). Vessel cargo containerization was introduced in the 1950s, and has improved the efficiency of marine transportation of goods globally (Levesque, 2011). According to the United Nations Conference on Trade and Development, the volume of global containerized trade more than tripled between 1990 and 2021 and is expected to continue to rise as consumer demand increases and global markets expand (United Nations, 2022).

Passive acoustic monitoring is the traditional method for measuring underwater noise levels in the ocean, allowing for point source passive acoustic measurements of ambient noise, with contributions from sound sources 1000s of km away depending on the frequency and source level of the sound source (Andrew et al., 2011; Mckenna et al., 2009; Hildebrand, 2009; McDonald et al., 2006). Passive acoustic monitoring has been conducted in the ocean only post-industrial revolution; therefore, the ancient underwater sound levels under which marine invertebrates, fish, and mammals have evolved are poorly understood. Modeling is required to estimate pre-industrial soundscapes across the vast spatial scales of the ocean (Sertlek et al., 2019; Erbe et al., 2021; Farcas et al., 2020). In this study, we modeled pre-industrial underwater noise levels as wind-driven and compared them to modern ocean noise levels, which included contributions from wind and ships.

We chose the Santa Barbara Channel (SBC) for this analysis because it supports the transportation of cargo to and from the busiest shipping ports in the United States, the Port of Los Angeles and the Port of Long Beach (United Nations, 2022). Commercial shipping has risen over the past several decades, which has increased ocean noise levels in the Southern California Bight (Andrew et al., 2011; McDonald et al., 2006; Hildebrand, 2009; Mckenna et al., 2009). In addition to shipping, this region encompasses the Channel Islands National Marine Sanctuary, a hub of rich biodiversity and wildlife (Checkley and Barth, 2009). It serves as a crucial foraging ground for the endangered northeastern pacific blue whale (Calambokidis et al., 2015; Szesciorka et al., 2020). The human-wildlife interactions that are present and increasing in this region are noteworthy and merit further investigation.

The sound levels and temporal variability of underwater noise in the SBC have been investigated with passive acoustic moorings providing point source measurements, however additional analysis is needed to estimate noise increases relative to pre-industrial conditions (Hildebrand, 2009; McDonald et al., 2006; Mckenna et al., 2009). Moreover, the spatial variability of noise in the SBC has been previously explored by modeling noise due to shipping over the duration of a three month period (Redfern et al., 2017). However, spatiotemporal variability of

* Corresponding author at: 8622 Kennel Way, La Jolla, CA 92037-0205, USA.
E-mail address: vmzobell@ucsd.edu (V.M. ZoBell).

https://doi.org/10.1016/j.marpolbul.2024.116379
Received 29 November 2023; Received in revised form 10 April 2024; Accepted 13 April 2024
Available online 20 April 2024

ocean noise that takes into account a broader range of biologically relevant temporal and spatial scales are needed (Sertlek et al., 2019). No studies have been conducted in this region to quantify the spatiotemporal variability of pre-industrial ocean noise levels in comparison to modern ocean noise levels.

Estimation of pre-industrial baseline noise levels and comparison to modern noise measurements allows identification of regions that have been most impacted by ship noise and those less impacted. Understanding the spatiotemporal variability of present day underwater radiated ship noise is required for the development of focused and effective management and conservation strategies for marine mammals, fishes, and invertebrates, as these species utilize various regions of the SBC during different times of the year.

2. Methods

We examined pre-industrial and modern ocean noise levels in the SBC for the month of August 2017, an important summer foraging month for the endangered northeastern pacific blue whale (Burtenshaw et al., 2004; Szesciorka et al., 2020). A United States Coast Guard enforced and International Maritime Organization approved Traffic Separation Scheme (TSS) guiding north and southbound commercial vessels intersects with the blue whale biologically important feeding area (BIA) and Channel Islands National Marine Sanctuary (CINMS, Fig. 1) in this region. We modeled pre-industrial and modern noise at four time resolutions: hourly ($n = 744$), daily ($n = 31$), weekly ($n = 4$), and monthly ($n = 1$), to compare differences in excess noise over different timescales. Models were based on local wind speed estimates, real vessel transit data, and vessel-specific source level estimates. Pre-industrial (wind-driven) and modern (wind-driven + vessel-generated) noise were modeled at 50 Hz and 1 kHz with 2 × 2 km resolution within a bounding box which includes the SBC and CINMS (DD latitude 33.80°N to 34.70°N and DD longitude 118.83°W to 121.22°W).

The noise model was compared with 744 h of acoustic recording data collected at two sites in the SBC (Site B: 34.28°N, 120.03°W; Site C: 34.32°N, 120.81°W) during the modeled period (Fig. 1). These acoustic data were collected using High-frequency Acoustic Recording Packages (HARPs, Wiggins et al., 2007). The HARP was equipped with an omni-directional hydrophone suspended 10 m above the seafloor. HARP hydrophone electronics were calibrated at Scripps Institution of Oceanography and representative hydrophones were calibrated at the U.S. Navy's Transducer Evaluation Center facility in San Diego, California. Recordings were collected at sampling rates of 200 kHz (Site B) and 320 kHz (Site C).

To test the accuracy of the model, sound pressure levels at the depths of the acoustic sensors (Site B: 580 m; Site C: 750 m) were calculated for comparison with the measured data. Sound pressure at 30 m depth was also determined, as an approximation for the depth of singing blue whales in previous studies (Oleson et al., 2007; Redfern et al., 2017). Modeling largely mirrored the approach outlined in Erbe et al. (2021, Appendix A), with general methods and key differences highlighted below. Key differences include the resolution of the grid, radial length, model depth and frequency, as well as regional properties, all of which were altered to optimize modeling for the Santa Barbara Channel.

2.1. Wind data

To map the pre-industrial ocean noise levels driven by wind, hindcast wind speed estimates were obtained from the Cross-Calibrated Multi-Platform (CCMP) wind vector analysis product (Ricciardulli and National Center for Atmospheric Research Staff, 2022), as well as from local wind speed measurements from a National Oceanic and Atmospheric Administration (NOAA) buoy (station 46053) in the SBC. The CCMP wind analysis is a gridded dataset of surface winds from satellite microwave measurements combined with a background reanalysis field in 6-hour temporal and 0.25 degree spatial resolution. The NOAA buoy data had a temporal resolution of 1 h. The power spectral density of ocean noise as a function of wind speed was computed using the empirical model of Hildebrand et al. (2021) at 50 Hz and 1 kHz. The power spectral density was calculated for each grid cell at each of the three model depths (30, 580, 750 m).

2.2. Ship data

Automatic identification system (AIS) data were collected from an antenna on Santa Cruz Island serviced by the Santa Barbara Wireless Foundation, and compiled to produce hourly logs of ship occurrence over the modeled period (Fig. 1, sbwireless.org). The detection range of the AIS data is dependent on coastal temperatures, which affect the propagation of the AIS signal, and height of the transmitting antenna on the vessel. Typically, the receiving antenna has a detection range of 300 to 400 nautical miles (555 to 740 km) to the ship, allowing for good coverage within the study area (Fig. 1).

Ships were classified into eleven categories: Fishing, Tug, Naval,

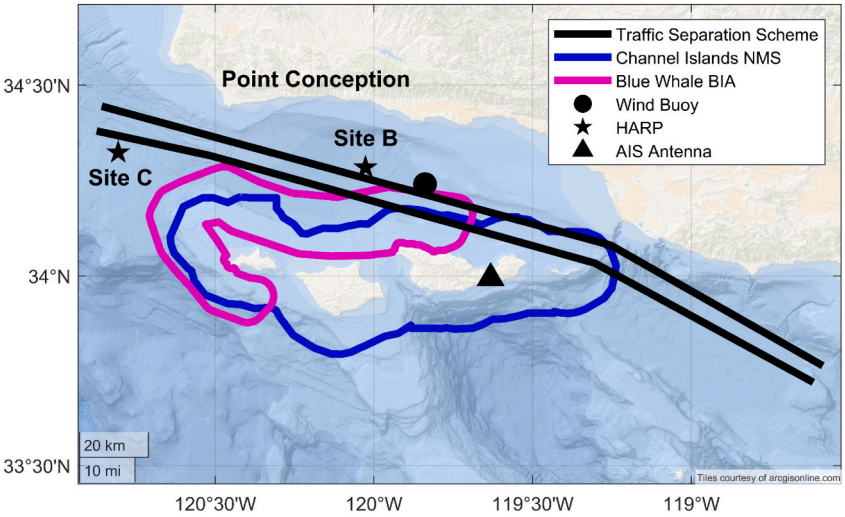

Fig. 1. Map of study area in the Santa Barbara Channel with traffic separation scheme shown with black lines, Channel Islands National Marine Sanctuary boundary in blue, and blue whale biologically important area (BIA) in magenta. High-frequency Acoustic Recording Packages (stars), wind buoy (dot), and AIS antenna (triangle) are labeled with black markers. (For interpretation of the references to color in this figure legend, the reader is referred to the web version of this article.)

Recreational, Government/Research, Cruise, Passenger, Bulker, Containership, Tanker, and Other. The categorization was based on the AIS ship type number, ship speed, and ship length, using the method of Macgillivray and de Jong (2021). Notably, the AIS records do not distinguish vehicle carriers, causing them to be grouped within the Bulker and Containership types. Ships that did not specify their type in the AIS logs were labeled as "Other". Stationary ships (those with an AIS speed equal to 0 knots) were excluded from the data compilation.

The model for estimating noise generation from commercial shipping in the SBC region was developed through a detailed analysis of ship movements. This process involved linearly interpolating ship tracks to a one-minute temporal resolution within a 2×2 km spatial grid. Each grid cell could act as an acoustic source when occupied by one or more moving ships. Using the AIS records, an hourly map was generated to pinpoint source cells containing ships. The latitude and longitude of activated source cells, the duration (in minutes) for which ships were present within the source cells, and the attributes of the vessels (type, speed, and length) were used to estimate the acoustic source characteristics for each cell. Subsequently, every activated cell was integrated into a propagation loss model (described in Section 2.5), to calculate the spatial distribution of the sound energy emitted.

2.3. Vessel source level model

To model the noise radiated from a ship over long ranges, the Monopole Source Level (MSL) of the vessel is required. The MSL of a vessel is dependent on numerous factors including characteristics of the vessel as well as prevailing oceanographic conditions (McKenna et al., 2013; Simard et al., 2016; Gassmann et al., 2017; Chion et al., 2019; MacGillivray et al., 2019; ZoBell et al., 2021; ZoBell et al., 2023). Several models have been developed to estimate vessel-specific MSLs using these characteristics, although substantial uncertainties and variabilities remain (Breeding et al., 1996; Macgillivray and de Jong, 2021).

We used the MSL model for vessels from the Joint Monitoring Program for Ambient Noise in the North Sea (JOMOPANS), developed using the Enhancing Cetacean Habitat and Observation (ECHO) dataset (Macgillivray and de Jong, 2021). The model estimates frequency-dependent MSL based on ship speed, length, and ship class. In our study, we employed this model to estimate vessel-specific MSLs at 50 Hz and 1 kHz.

The ship-type composition and speeds that were used to develop the JOMOPANS model are different from those found within the SBC. Therefore, we made adjustments to the MSL model to better reflect the ships in the SBC region. In particular, we adjusted the total reference length for an average ship and the reference speed for each ship type. The JOMOPANs model defines an average ship to have a length of 91.4 m, whereas the average ship in our study was 170.1 m. Additionally, the reference speeds per vessel class were modified to equal the average speed for vessels in our study (Supplemental Table 1). MSLs for each ship class adapted from the JOMOPANS model are shown in Supplemental Fig. 1.

2.4. Acoustic properties of the water column and sea floor

Acoustic properties of the water column and the seafloor were required for propagation loss modeling. Temperature and salinity profiles were obtained from the Short-term California State Estimation (ecco.ucsd.edu/case.html) ocean model in 1/16 degree spatial resolution at 72 depths between the surface and 2000 m. Sound speed profiles were calculated from these data with the nine-term equation for sound speed in the ocean of Mackenzie (1981).

Bathymetric data were obtained from the General Bathymetry Chart of the Oceans (GEBCO Compilation Group, 2023), with a spatial resolution of 15 arc-seconds. From the bathymetry data, the slope angle of the ocean floor was calculated as the arctangent of the magnitude of the gradient. Three acoustic floor types were identified from the bathymetry and slope angle: shelf, slope, and basin. Shelf was defined as regions where the bathymetry was less than or equal to 200 m deep and the slope angle was less than or equal to 0.75 degrees. Slope was defined as regions where slope angle was greater than 0.75 degrees. Basin was defined as regions where depth was greater than 200 m and slope angle was less than 0.75 degrees.

Sediment cores were taken at the seafloor using a gravity corer and a multi-corer (Blomqvist, 1991). Cores were collected at three sites to represent the basin, slope, and shelf bottom types (Fig. 2). Gravity cores were taken from the slope and basin sites and were sectioned, capped, and stored for compressional wave speed measurements in the following weeks in the lab. A gravity core was attempted at the shelf site but was unsuccessful, as it was unable to penetrate the sediment. A multi-corer was successfully able to penetrate the sediment at the shelf site and compression wave speed measurements were taken onboard the ship directly after retrieving the sample.

Compressional wave speed was estimated from core sediment by measuring the distance a sound wave travels through the sediment and the time taken to travel the distance, based on methods from Boyce (1973). To achieve this, a sediment subsample was taken from the cores. Sound velocity was measured for each sample using a Krautkramer Branson USD10 Ultrasonic Digital Flaw Detector and two Krautkramer Branson longitudinal acoustic transducers (Alpha series, 10·MHz, 0.25·mm; Krautkramer, General Electric Inspection Technologies, Hverth, Germany) attached to digital calipers (model no. CD-8″CS, Mitutoyo America Corp., Aurora, IL, USA). The Krautkramer velocimeter system measured the transmission time of 10·MHz broadband pulses. The calipers measured the sample thickness to the nearest millimeter, and velocity was calculated by dividing the thickness by the travel time. Prior to measuring the samples, the velocimeter was calibrated using distilled water at room temperature (22.5 °C), assuming a sound speed of 1490 m/s (Chen and Millero, 1977).

The sediment compressional wave speeds were 1485, 1500, and 1520 m/s for the basin, slope, and shelf sites, respectively. Surface sediment was mostly organic matter and clay (basin), silty clay (slope), and fine sand (shelf). Compressional wave speed and density at deeper sediment depths were taken from the Ocean Discovery Program's drilling data (Site 893 Hole A) in the SBC (Carson et al., 1992). The depth of the seismic basement was determined from sediment thickness which was gathered from the Total Sediment Thickness of the World's Oceans and Marginal Seas Database (GlobSed version 3, Straume et al., 2019).

2.5. Source-receiver propagation loss

For each source cell activated by a ship transit, radials were cast in 10-degree intervals from the central latitude-longitude point to a maximum range of 40 km. The bathymetric profile along each radial was determined with 500 m resolution. Radials were halted if they intersected land. To determine the sound propagation loss (PL) along the radial, a range-dependent parabolic equation method, RAMGEO (Collins, 2001), was used at 50 Hz and 1 kHz with 10 m range and 5 m depth resolution. PL was then interpolated to a 1 m depth and range resolution. Range-dependent sound speed profiles, sediment properties, and depth to the seismic basement were incorporated into the model. The parabolic equation method is a far-field approximation. For some frequencies, the model experiences distortions in the near-field (0–2 km) when the propagation angle approaches the vertical (Wang et al., 2014). To correct for model distortions found in the near-field approximations for the mid-frequency (1 kHz), the minimum PL at each depth was extended from the range of minimum PL value backwards to the center of the radial (range = 0 m). The source depth for all ships was 5 m since that is the average depth of propeller-cavitation in this region. Illustration of propagation loss radials at 50 Hz and 1 kHz are shown in Fig. 3. Note that at 50 Hz sound propagates within the sediment, whereas there is little sediment sound propagation at 1 kHz. The PL was extracted at the depth of each acoustic measurement sensor (Site B: 580 m, Site C:

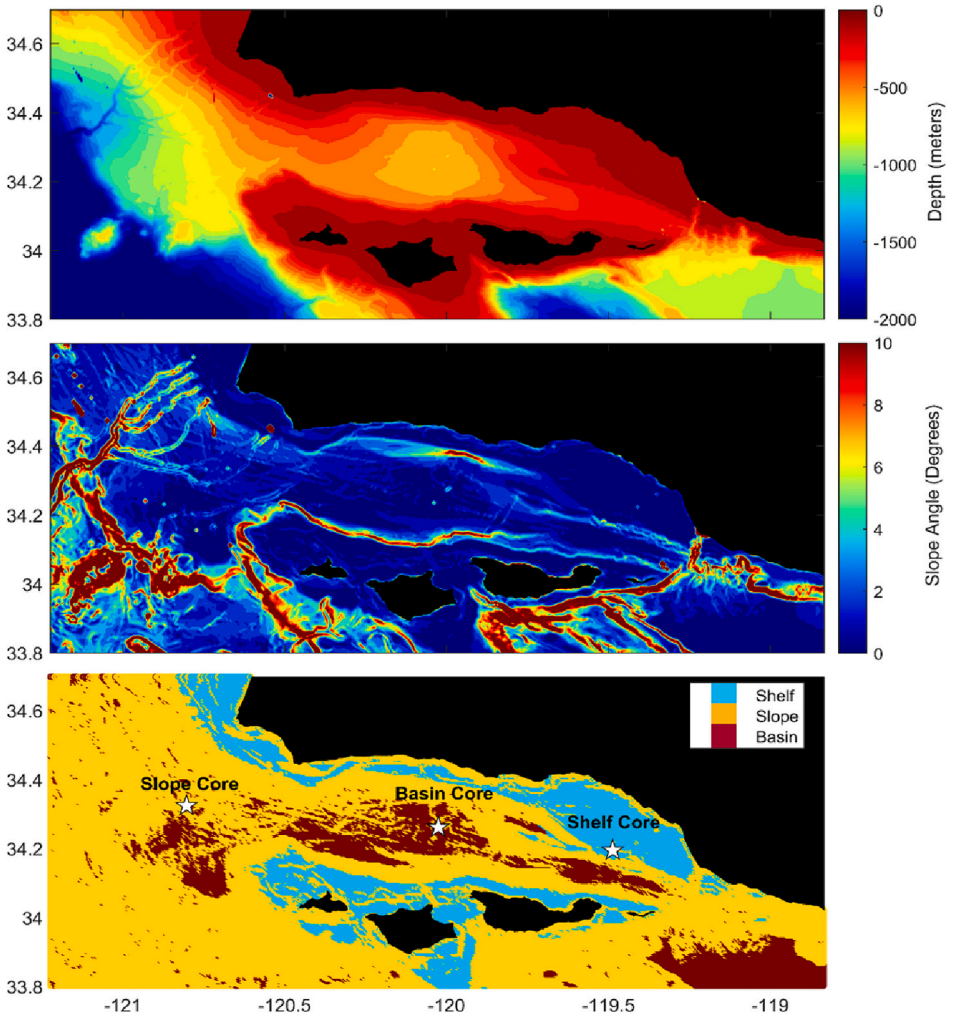

Fig. 2. Acoustic seafloor types in the Santa Barbara Channel identified by bathymetry (top) and slope angle (middle) data. Zones identified in this analysis are identified (bottom) as shelf in blue, slope in yellow, and the basin in red. Sediment core locations are labeled with white pentagrams. (For interpretation of the references to color in this figure legend, the reader is referred to the web version of this article.)

750 m) as well as at 30 m.

2.6. Sound pressure level for shipping

The contribution of each ship in the study area was integrated to calculate their cumulative sound pressure level (SPL). During each hour, ships with unique source levels were treated sequentially. Source cells, those containing ships, were assigned an SPL at 1.0 km range from the vessel, the mean distance between two random points inside the source cell (Erbe et al., 2021). The duration T (in seconds) that a ship with corresponding source level was present within each cell was added to estimate sound exposure level (SEL) within the cell. For grid cells not at the source, the PL was subtracted from the source level along each radial, for each assessed depth. Hourly SPL (dB re 1 μPa^2 / Hz, Eq. (1)) was then calculated by accounting for the duration of exposure, and the number of seconds in 1 h, as follows:

$$SPL = SL + 10^{*}log10(T) - PL - 10^{*}log10(60^{*}60) \quad (1)$$

The hourly SPL was subsequently converted from polar coordinates to Cartesian coordinates to enable interpolation onto the 2 × 2 km grid at each depth. Using the Cartesian grid, the SPL values were cumulatively summed over each activated source cell to yield the total SPL for all ships within the study area for each hour.

2.7. Comparison of measured and modeled ocean noise levels

Hourly SPLs from the field acoustic measurements were compared with hourly estimates from the modern noise model. Long-Term Spectral Averages (LTSAs) were calculated for the field acoustic measurements in 1 Hz frequency bins over 5 s time bins (Wiggins and Hildebrand, 2007), followed by averaging these into hourly SPLs at 50 Hz and 1 kHz. These measured SPLs were then compared with the modern noise model. The modern noise model at Site B was estimated as the incoherent linear sum of ship noise sources, and noise based on wind data from the adjacent NOAA buoy station. Wind model estimates were found to be less accurate on hourly scales at Site B than local buoy data due to the influence of nearby topography. The modern noise model at Site C, which is not island-adjacent, incorporated the CCMP wind model. Differences in dBs between the measured and modeled SPLs were quantified on an hourly basis to assess the accuracy of the model.

2.8. Comparison of pre-industrial and modern ocean noise levels

Modeled pre-industrial and modern ocean noise estimates were also compared. The pre-industrial ocean noise model was based solely on noise generated by the wind. Modern noise was calculated from an incoherent linear sum of the wind-generated and ship-generated sound pressure levels, with subsequent conversion to dB. Excess noise, defined

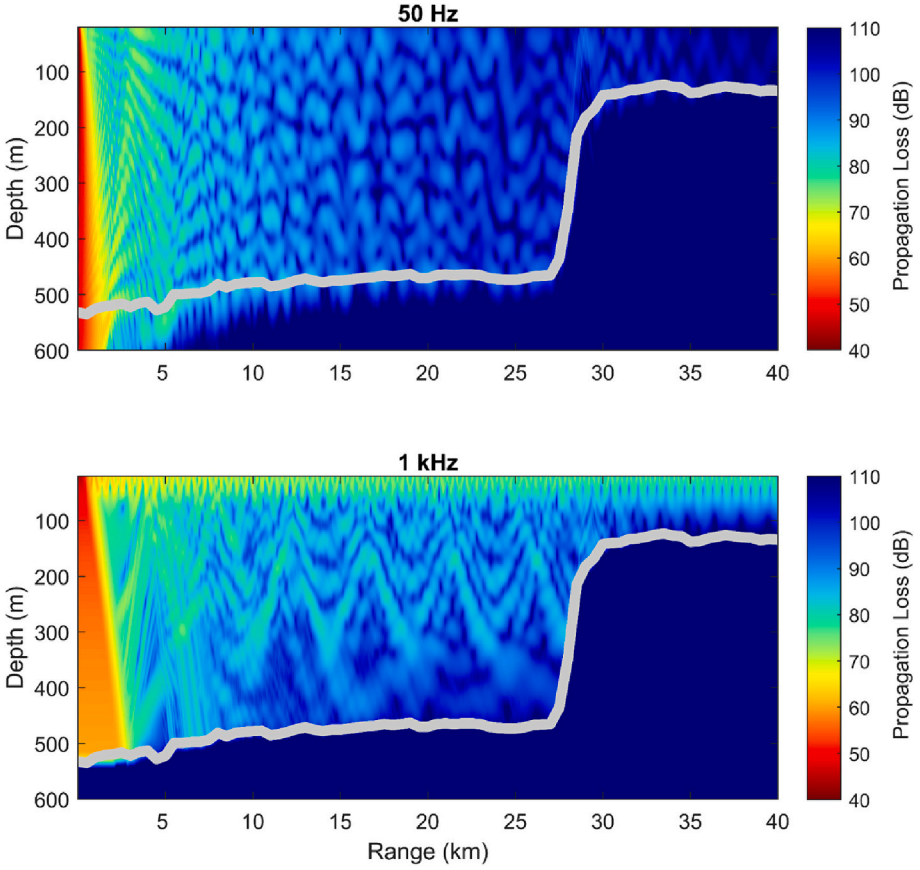

Fig. 3. Propagation loss at 50 Hz and 1 kHz as a function of range (km) and depth (meters) for a grid cell with center point at 34.29°N and 120.14°W. Red corresponds to lower propagation loss (40 dB) and blue corresponds to high propagation loss (110 dB). Gray lines show bathymetric depth. (For interpretation of the references to color in this figure legend, the reader is referred to the web version of this article.)

as the amount by which modern noise levels exceed pre-industrial noise levels, was calculated across four temporal resolutions (hourly, daily, weekly, and monthly), all during the month of August 2017. Median, median absolute deviation, 5th percentile, and 95th percentile statistics were calculated for the hourly modern noise model.

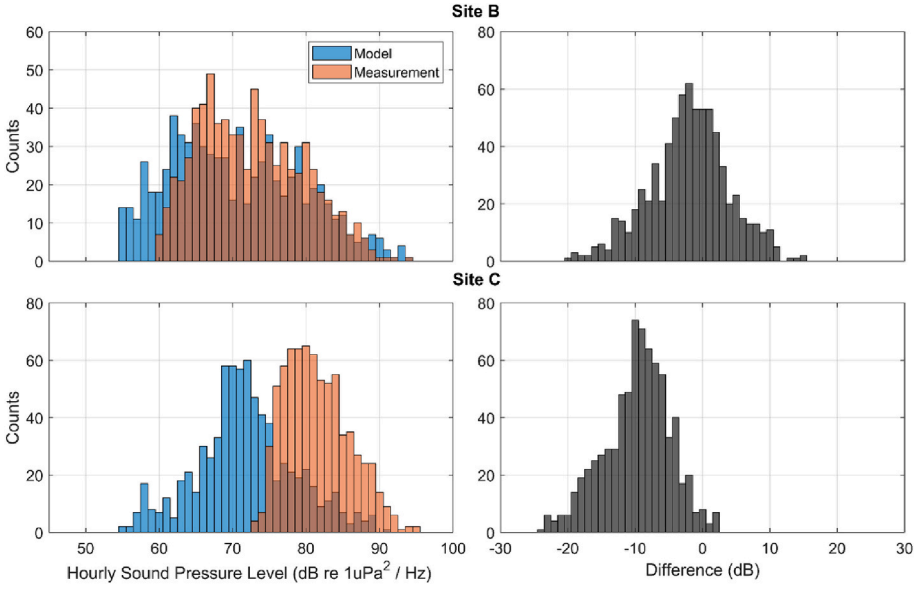

Fig. 4. Comparison of hourly low-frequency (50 Hz) modeled modern sound pressure levels (SPLs) with measured SPLs from in situ measurements at Site B (upper) and Site C (lower). Difference in dB reports the modeled minus the measured hourly SPLs. Number of hours $n = 744$.

3. Results

3.1. Comparison of measured and modeled ocean noise levels

3.1.1. Low-frequency

The measured hourly low-frequency (50 Hz) noise at Site B varied by an impressive 34.5 dB (59.9 to 94.4 dB re 1μPa^2/ Hz, Supplemental Fig. 2). This broad variability reflects periods of high noise when ships were nearby and low noise in the absence of local ships, with minimal exposure to distant vessel noise (Fig. 4). Modeled SPLs followed a similar pattern, and the median difference between the modeled and measured SPLs (modeled - measured) was −1.8 dB ± 4.6 dB. Good agreement was observed between the model and measured noise levels when ships were passing at close range and noise levels were high, however, the model tended to under-predict noise levels in the absence of ships when levels were low.

Measured low-frequency hourly noise at Site C varied by 22.6 dB (72.4 to 95.0 dB re 1 μPa^2 / Hz) and the measured SPLs were consistently higher than the model, suggesting that the model was not adequately capturing sources of noise observed at this site. The difference between the modeled and measured SPLs at Site C was −9.3 ± 3.9 dB (Fig. 4).

Across the region, median hourly SPL estimates were highest in the North West section of the grid, where there is less protection from wind and where the bathymetry is deep, allowing ship noise to propagate further (Fig. 5). Median SPL was lowest in the northeast corner of the map, which is occupied solely by small boats and where wind speeds are low. There were also slightly lower median SPL estimates south of Anacapa and Santa Cruz Island, where these islands may be shielding propagation of ship noise from within the shipping lanes. The median absolute deviation of hourly SPL is high along the shipping lane, with the maximum variability north of Anacapa Island. In the nearshore region, there was high median absolute deviation from small boats transiting to and from the Santa Barbara Harbor. The 5th percentile SPLs were highest in the northwest portion of the grid, arising from higher wind speeds in this area which contribute to higher SPLs. The 5th percentile SPL values ranged from 56.3 dB to 62.6 dB across the region. The area where the 95th percentile SPL values were highest extended out from the traffic separation scheme, and lowest in shallow water and regions shielded from the traffic separation scheme by the island. The 95th percentiles ranged from 57.9 dB to 92.8 dB. Areas with deeper bathymetry allowed for a greater spread of ship noise that extended into the 95th percentile.

3.1.2. Mid-frequency

At mid-frequency (1 kHz), a smaller variation in measured and modeled SPL values were seen at both sites than what was observed at low-frequency. Site B's measured SPLs varied by 20.1 dB, from 48.1 to 68.2 dB (Fig. 6). The median difference between modeled and measured levels was −1.3 ± 2.6 dB. This difference was primarily due to instances with measured SPL values that were higher than any of the modeled SPL values (Fig. 6).

Measured mid-frequency SPLs at Site C's varied by 19.4 dB, from 50.3 to 69.7 dB. The median difference of the measured data from the model was 0.1 ± 2.2 dB. At Site C, the pattern of more instances of higher SPL values from the measured data did not occur, however, too few instances of low noise were observed (Fig. 6).

The median mid-frequency SPL was highest in the North West section of the grid, where wind speed is the highest (Fig. 7). The median SPL was not the highest within the shipping lanes, displaying the significance of wind noise at 1 kHz frequency. Median SPL was lowest in the northeast corner of the study area, owing to the protection from high winds in this location due to the shape of the coastline. SPL variability was high along the shipping lane and in the southwest portion of the grid. The variability within the shipping lane was lower than for the 50 Hz model, and wind speed fluctuations were likely the cause of the higher variability in SPL in the southwest region. The 5th percentile (low noise) SPL values had little variation (52.7 dB to 58.8 dB) across the region. Whereas, the 95th percentile (high noise) SPL values had more than 21 dB variations (54.3 dB to 75.6 dB) and were highest along the traffic separation scheme. The 95th percentiles were lower in the northeast corner of the map which is only occupied by small boats and has low wind speeds. The 95th percentiles were also slightly lower south of Anacapa and Santa Cruz Island which may be shielded from ship noise.

3.2. Comparison of pre-industrial and Modeled Ocean noise levels

SPLs are mapped for the pre-industrial, modern, and excess noise models, and shown in hourly, daily, weekly, and monthly averages in Fig. 8 (50 Hz) and Fig. 9 (1 kHz) for the month of August 2017. The pre-industrial low-frequency (50 Hz) noise maps (Fig. 8) show a strong east-west gradient, with higher noise levels offshore and lower levels along the coastline, by as much as 10–15 dB in the example shown for one of the hourly averages, but by only 5 dB in the monthly average. This is consistent with the patterns of winds, predominantly from the west, and the shielding effect of the landmass for the eastern areas of the Santa Barbara Channel. The examples shown for the hourly and daily pre-

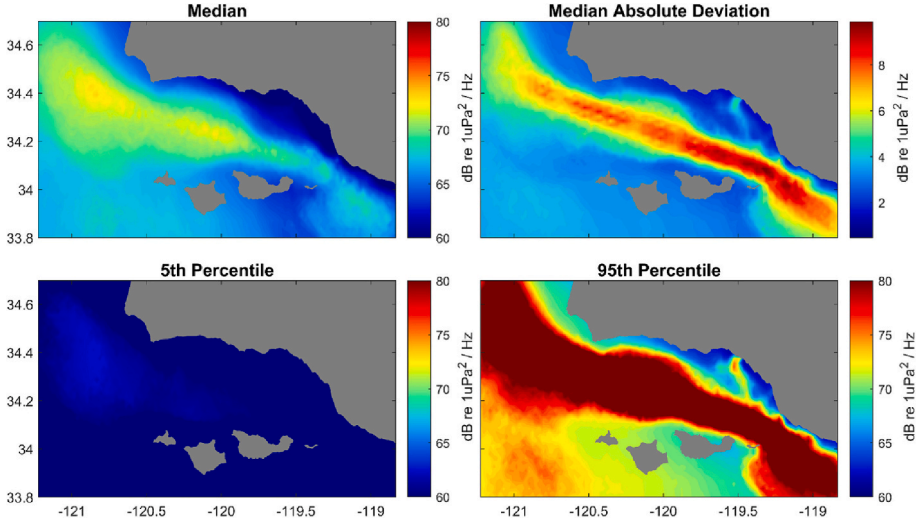

Fig. 5. Modeled hourly sound pressure levels from wind and ship noise at 50 Hz and 30 m depth as median, median absolute deviation, 5th percentile, and 95th percentile.

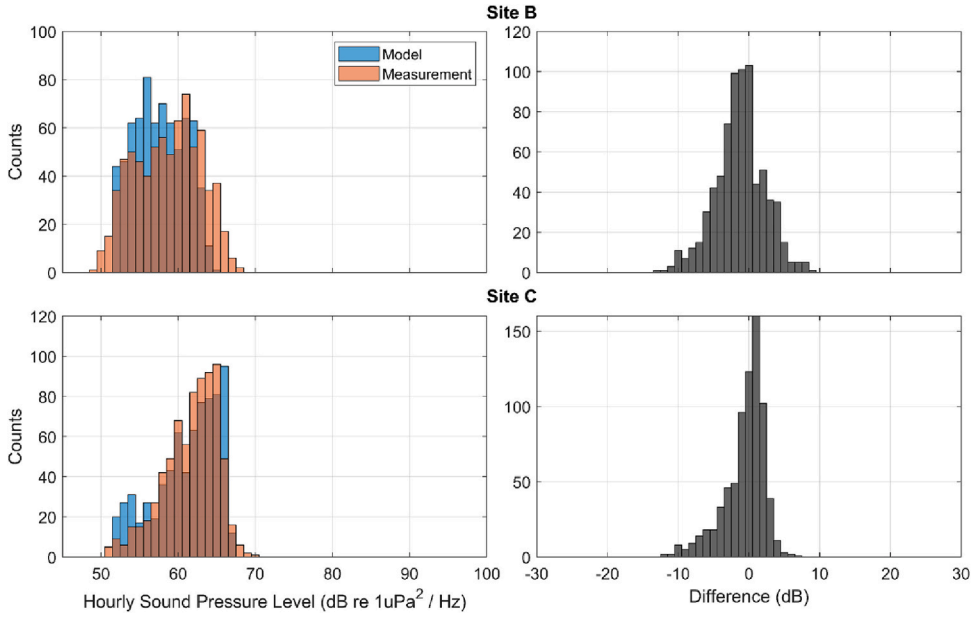

Fig. 6. Comparison of 1 kHz hourly (n = 744) modeled modern sound pressure levels (SPLs) with measured SPLs from in situ measurements at Site B and Site C. Difference in dB reports the modeled minus the measured hourly SPLs.

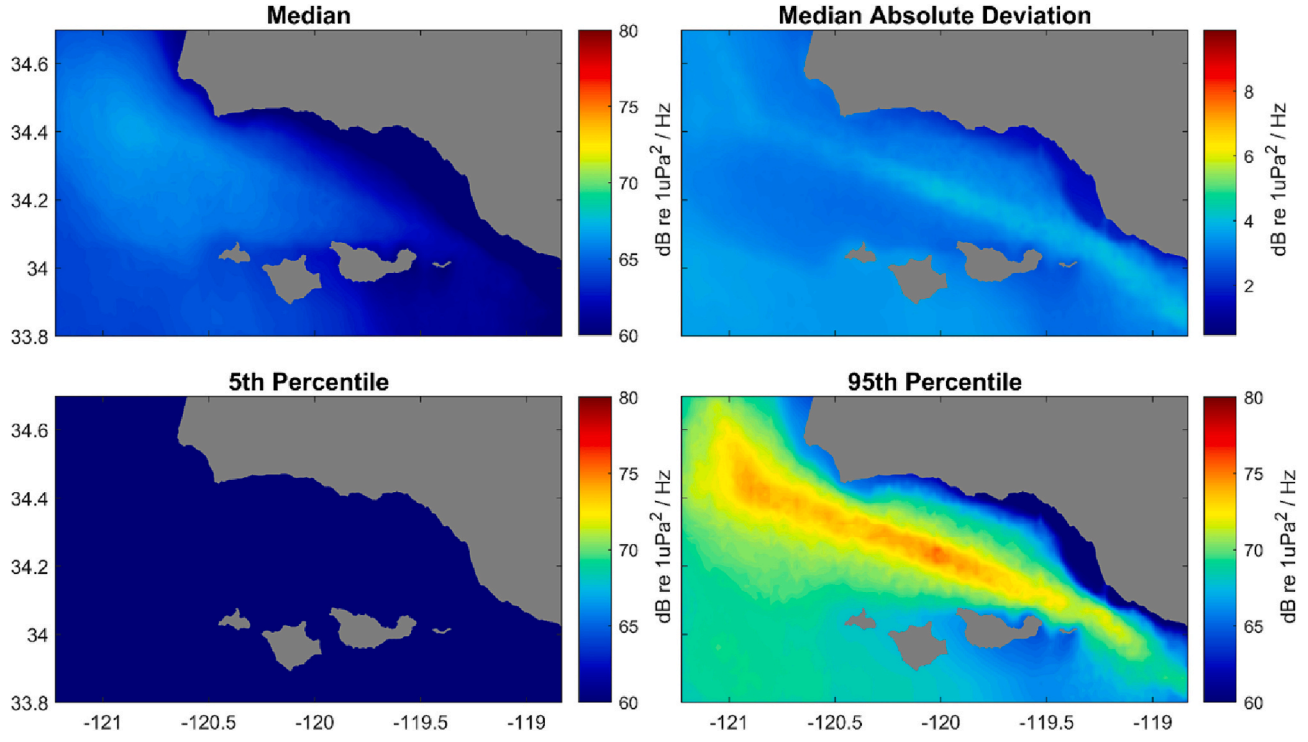

Fig. 7. Modeled hourly sound pressure levels at 1 kHz and 30 m depth as median, median absolute deviation, 5th percentile, and 95th percentile.

industrial noise are higher than the weekly and daily noise due to high wind speeds affecting short-term temporal resolutions that are averaged out in the longer-term temporal resolutions. The weekly and monthly pre-industrial noise maps do show some spatial gradient for wind noise, but are more uniform across the region than what can be observed in the hourly or daily averages.

In contrast, the modern low-frequency (50 Hz) noise map (Fig. 8) outlines the shipping lanes as a zone of high noise levels, as much as 10 dB higher than the surrounding areas. The differences are apparent in the excess noise map, which reveals the shipping lanes to be higher than the pre-industrial noise levels on all time scales. The maximum excess noise levels across the grid were 15.2 dB, 11.8 dB, 11.2 dB, and 11.5 dB for hourly, daily, weekly, and monthly temporal resolutions, respectively). The hourly time scale for modern and excess noise shows greater spatial heterogeneity than the daily, weekly, and monthly time scales. In the hourly temporal resolution, two ships are clearly seen in the shipping lane with additional small boats contributing to nearshore SPLs, near Santa Barbara Harbor and the Port of Hueneme. The presence of small boats is not as well seen in the daily, weekly, and monthly noise maps, as the small boat presence is averaged out over longer time scales. In the

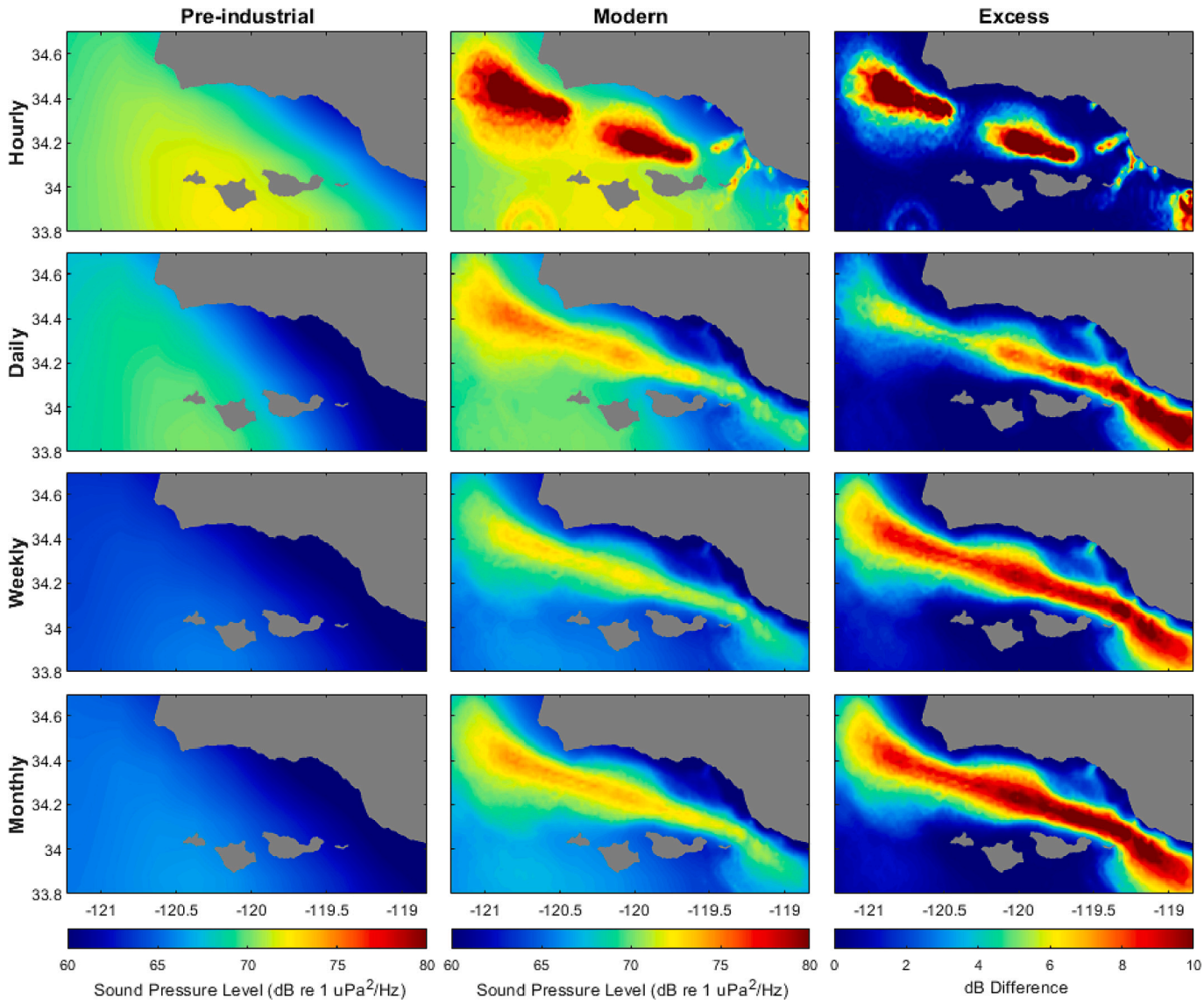

Fig. 8. Sound pressure levels at 30 m for 50 Hz pre-industrial (left) and modern (center) noise in hourly, daily, weekly, and monthly average time scales. Excess noise (right) shows modern noise minus pre-industrial noise. Hourly maps show hourly SPL from August 1, 2017 00:00:00 to August 1, 2017 01:00:00 (UTC). Daily maps show an average of hourly SPLs over the time range August 1, 2017, 00:00:00, to August 2, 2017, 00:00:00. Weekly maps show an average of hourly SPLs over the time range August 1, 2017 00:00:00 to August 8, 2017, 00:00:00. Monthly maps show an average of hourly SPLs over the entire month of August 2017. Note differences in color scale bars.

daily, weekly, and monthly temporal resolutions, the excess noise is mostly centered on the shipping lane, and extends farther away from the shipping lane in areas with deeper bathymetry, such as off of Point Conception and in the Santa Barbara Basin.

The mid-frequency (1 kHz) noise map had a maximum excess noise of 4.7 dB, 5.2 dB, 5.1 dB, and 5.3 dB for hourly, daily, weekly, and monthly temporal resolutions, respectively. The pre-industrial SPLs are greatest in the southwest section of the region due to higher wind speeds offshore. The majority of the excess noise was concentrated in the shipping lane for all temporal resolutions. Spatial heterogeneity of excess noise is seen in the hourly temporal resolution, whereas the heterogeneity is lost in the daily, weekly, and monthly sound levels. Excess noise levels at 1 kHz did not reach as high as those in the 50 Hz map.

4. Discussion

This study developed models comparing pre-industrial and modern ocean noise levels, as an aid to understanding the acoustic degradation resulting from commercial shipping. We modeled wind-generated noise as a proxy for pre-industrial noise, and ship noise plus wind noise to represent modern ocean noise levels. Our analysis was conducted for August of 2017 at two frequencies, 50 Hz and 1 kHz, the former low-frequency within the band of greatest impact from shipping and the latter mid-frequency with primary influence from wind noise and lesser shipping influence. Field measurements allowed assessment of the accuracy of the modern noise model.

4.1. Comparison of measured and modeled ocean noise levels

Good agreement between the modeled and measured noise values was found when ships were nearby, and when wind noise was dominant, with no other sound sources nearby. At times when the model was lower than the measured data, seen at both sites and frequencies (Fig. 4, Fig. 6), it was found that additional noise sources were present, such as ships that were not included in the AIS data, or machinery noises

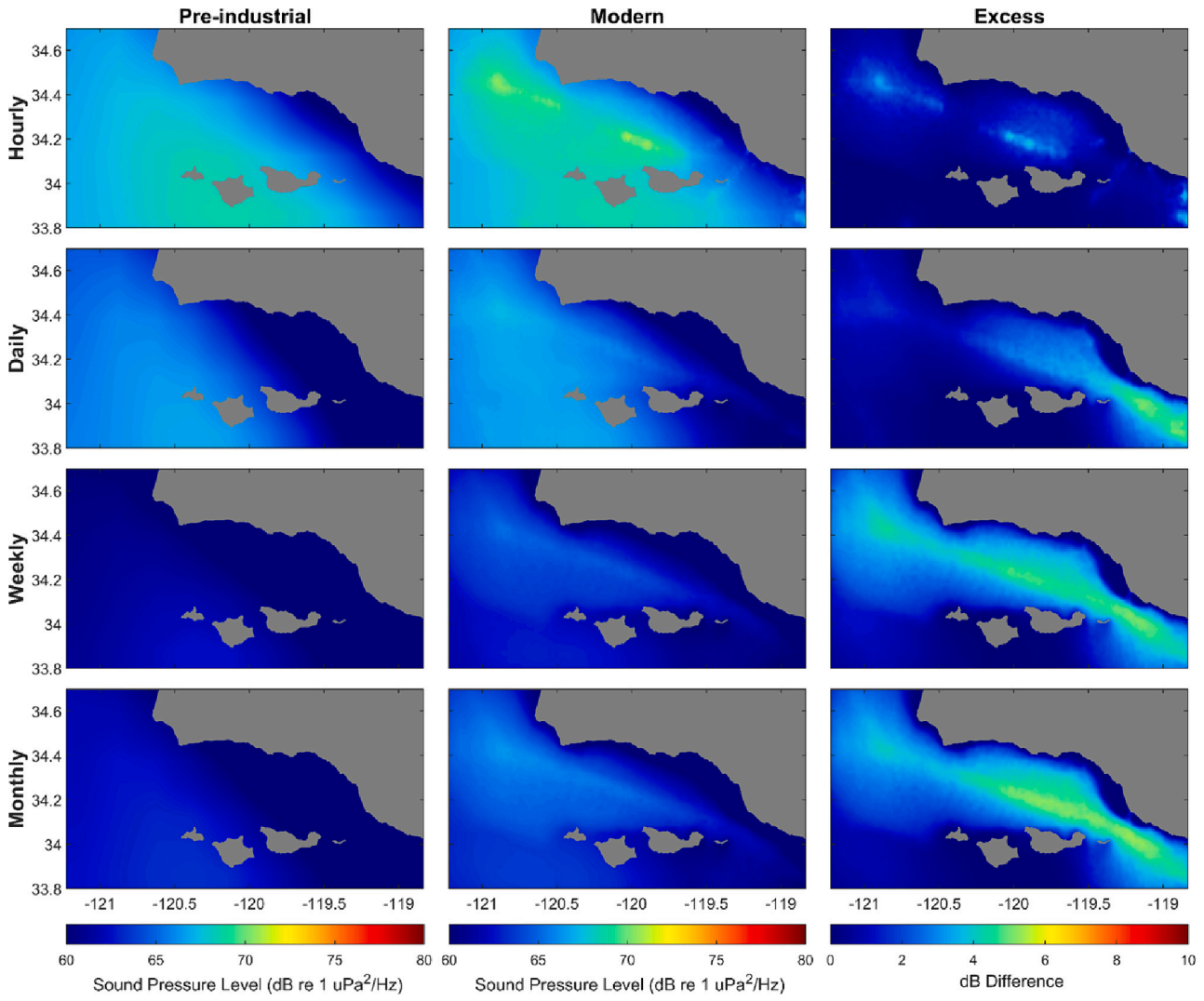

Fig. 9. Sound pressure levels at 30 m for 1 kHz pre-industrial (left) and modern (center) noise in hourly, daily, weekly, and monthly average time scales. Excess noise (right) shows modern noise minus pre-industrial noise. Maps use the same time ranges for the temporal resolutions as Fig. 8. Note differences in color scale bars.

generated from stationary ships located near the measurement site. Baleen whale vocalizations were another sound source not included in the models that contributed to these discrepancies (Supplementary Fig. 3). This mirrors findings in sound mapping projects in the Australian EEZ (Erbe et al., 2021), and highlights the importance of future models incorporating natural biological sounds to increase model precision.

At the recording site located inside the SBC basin (Site B), there was good agreement between measured and modeled noise, with a median difference within 1–2 dB between them at 50 Hz. This is an improvement from previous work which had a difference of 11 dB between model and measured SPLs for 50 Hz at Site B. However, the model for 50 Hz at Site C, located off of Point Conception, was consistently ~9–10 dB lower than the measured data suggesting that an un-modeled source of noise was present in the measurement data. The consistent underestimation of the noise model at Site C is likely explained by the influence of noise from long-range shipping in much of the North Pacific, which was not included in our modeling effort. Improved model estimates at Site C might be achieved by incorporating a wider area of the North Pacific in the model.

For mid-frequency (1 kHz) model estimates, there was good agreement at both Site B and Site C (within 2 dB). At Site B, there were hours in which the measured data were higher than the modeled data. This is likely due to wind being the dominant source of noise at the 1 kHz frequency. The buoy used for wind speed measurements and subsequent wind noise calculations was approximately 10 km east of Site B. The wind buoy may have been recording wind speeds that were lower than the wind speeds that occurred at the Site B recording location, making the modeled SPLs lower than the measured SPLs. When attempting to use the CCMP model for the wind noise calculations at Site B, greater disagreements between the model and measured SPL values were introduced, likely due to difficulties in predicting wind speeds surrounded by land masses. Deploying a wind buoy closer to Site B or developing a wind speed model that incorporates additional buoy data may be necessary to achieve higher accuracy wind speed data in time and space within the SBC.

4.2. *Comparison of pre-industrial and modeled ocean noise levels*

Based on our modeling, modern underwater noise levels were higher than pre-industrial levels within the study area. The excess noise levels extended beyond the traffic separation scheme and into the nearshore regions of the Santa Barbara Channel. The excess noise expanded away from the shipping lanes more in deeper waters, such as off Point Conception. The region between the mainland and Anacapa Island had the highest intensity of excess noise in both frequency bands, most likely because of the small corridor that yields high congestion of ships in this area, as well as the narrow, steep-walled bathymetry that reflects noise, containing it within a small region. Differences between pre-industrial

and modern ocean noise levels were greatest at the hourly time resolution for 50 Hz, and varied when averaging over different temporal resolutions.

Unlike sound mapping investigations in the Australian EEZ, our study had high proportions of area with excess noise from shipping, which is comparable to studies in northern hemisphere oceans (Farcas et al., 2020; Sertlek et al., 2019). In the Northeast Atlantic, excess noise was greatest for the low-frequency (63 Hz) model in comparison to higher frequency models (Farcas et al., 2020). Deeper waters in the northern North Sea allowed for ship noise to propagate further, similarly to the region off of Point Conception in this study (Farcas et al., 2020). Time window averaging in this study parallels findings in Sertlek et al. (2019), with higher sound levels indicated for shorter time resolutions. This underscores the criticality of selecting ecologically and biologically relevant time windows for acoustic analyses.

4.3. Limitations and uncertainties

The limitations and uncertainties of these models are still of concern, despite the extensive data and the care that went into their construction. For instance, errors in AIS data such as vessels without an AIS antenna or false AIS signals may lead to errors within our modern noise model. Container ships are the dominant vessel type in the region, therefore lacking more detailed information, we used a static representative source depth of 5 m for all vessels (Erbe et al., 2021). This is deeper than the propeller depths of smaller vessels, which typically have effective source depths of 1–2 m. Improving estimation of vessel specific source depths, and incorporating these different depths into the model would likely improve model noise estimates. The model described here was run on a desktop computer, however, to incorporate computationally expensive details including greater vessel specificity, future models will likely require more advanced computing infrastructure.

This modern noise model utilized an MSL model developed from ship measurements from the Enhancing Cetacean Habitat and Observation (ECHO) dataset (Macgillivray and de Jong, 2021). Although there were large sample sizes for some of the ship types included in the model, these vessel specifications may be different from the ships that transit the SBC. The ships found within the SBC were on average larger than the average ship used in the JOMOPANS model and also had different reference speeds for each ship type. Creating an MSL model from the ships within the SBC for ship noise mapping in the same region may improve model accuracy. The JOMOPANs model has a statistical uncertainty of 6 dB (Macgillivray and de Jong, 2021), which may have contributed to disagreements between the modern noise model and measured data in our study. Including additional variables that are known to affect source levels, such as oceanographic variables, may help increase MSL model accuracy. Investigating new ways to develop MSL models using machine learning algorithms may be an effective approach to reduce uncertainty.

Modeled and measured data were explored for the month of August, as this is an important foraging time for the endangered northeastern pacific blue whale. Exploring variability both in anthropogenic noise and geophysical noise will be interesting to investigate for different months and seasons. Specifically, shipping traffic may display certain seasonal patterns, environmental conditions such as stratification may affect sound speed profiles, and wind speeds may increase or decrease depending on the season. All of these factors may affect baseline noise conditions for pre-industrial and modern sound levels and should be explored further with time series analyses.

4.4. Implications for management

Many marine organisms, including fish and mammals, are motile and not constrained to one location over the course of a month and may experience a variety of different acoustic soundscapes throughout the duration of a season. Modeling noise levels in short temporal resolutions is important to capture the heterogeneity of the soundscape over time (Sertlek et al., 2019). The changes in soundscape over short time scales (hours / days) may be important when answering questions about movement and behavior, while longer time scales (weeks / months) may be more helpful when investigating physiological questions such as organism stress levels.

Ship noise reduction has been identified as a priority of the International Maritime Organization and International Whaling Commission (Chou et al., 2021). The model developed here has the potential of not only analyzing past and current ocean noise levels but also modeling noise under future management scenarios such as different shipping solutions and mitigation strategies. Modeling different mechanisms of noise reduction (vessel slow downs, design, routing) may be an effective approach to allow managers to select certain techniques rather than others. Comparison of current and future management scenarios to a pre-industrial baseline can inform discussions of the noise-related benefits and tradeoffs of proposed approaches. Simulating ocean soundscapes with AIS data is valuable for understanding how best to reduce ship noise and select the most effective solutions.

5. Conclusion

This study develops a model to compare pre-industrial ocean noise levels versus modern noise levels within the Santa Barbara Channel region. In situ validation shows good agreement between measured ocean noise levels and modeled ocean noise levels in certain areas and conditions. This underscores the significance in accounting for additional noise sources and acoustic properties for ongoing validation and refinement. Model predictions may be used to identify areas that have been acoustically degraded for targeted conservation and management efforts. Simulations of noise reduction strategies through modeling may aid in identifying the most efficient strategies to reduce underwater noise pollution in heavily trafficked areas.

Supplementary data to this article can be found online at https://doi.org/10.1016/j.marpolbul.2024.116379.

CRediT authorship contribution statement

Vanessa M. ZoBell: Writing – review & editing, Writing – original draft, Validation, Software, Methodology, Investigation, Funding acquisition, Formal analysis, Conceptualization. **John A. Hildebrand:** Writing – review & editing, Supervision, Investigation, Conceptualization. **Kaitlin E. Frasier:** Writing – review & editing, Supervision, Investigation, Conceptualization.

Declaration of competing interest

The authors declare that they have no known competing financial interests or personal relationships that could have appeared to influence the work reported in this paper.

Data availability

Data will be made available on request.

Acknowledgements

This work was funded by the Dr. Nancy Foster Scholarship, the Office of National Marine Sanctuaries, the Green Family Fellowship, and the UCSD Science Policy Fellowship. Support for field data collection was provided by the National Aeronautics and Space Administration Biodiversity and Ecological Forecasting program (NASA Grant No. NNX14AR62A), the Bureau of Ocean and Energy Management Ecosystem Studies program (BOEM award No. MC15AC00006), and NOAA in support of the Santa Barbara Channel Biodiversity Observation Network. We thank Robert Miller and other members of the SBC MBON project. We thank Bruce Thayre, Kieren Lenssen, John Hurwitz, Erin

O'Neill, and Shelby Bloom from the Marine Bioacoustic Research Collaborative for help in data collection and processing. We want to thank the UC Ship Funds Program for use of the R/V Robert Gordon Sproul, and give special thanks to Mo and Paul Walczak, Margaret Morris, Alex Hangsterfer, and the science team and crew of SP2221 for training, support, and technical expertise in sediment coring and analysis. Finally, thanks to the crew of the R/V Shearwater for long-term support of HARP deployments and recoveries at Site C and Site B.

References

Andrew, Rex K., Howe, Bruce M., Mercer, James A., 2011. Long-time trends in ship traffic noise for four sites off the North American west coast. J. Acoust. Soc. Am. 129 (2), 642–651. https://doi.org/10.1121/1.3518770.

Blomqvist, S., 1991. Quantitative sampling of soft-bottom sediments: problems and solutions. Mar. Ecol. Prog. Ser. 72 (3), 295–304. https://doi.org/10.3354/meps072295.

Boyce, Robert, 1973. Appendix I: Physical Properties - Methods. College Station.

Breeding, J. Ernest, Lisa, J.R., Pflug, A., Bradley, Marshall, Walrod, Melanie Hebert, Mcbride, Walton, 1996. Research Ambient Noise Directionality (RANDI) 3.1 Physics Description.

Burtenshaw, Jessica C., Oleson, Erin M., Hildebrand, John A., McDonald, Mark A., Andrew, Rex K., Howe, Bruce M., Mercer, James A., 2004. Acoustic and satellite remote sensing of blue whale seasonality and habitat in the Northeast Pacific. Deep-Sea Res. II Top. Stud. Oceanogr. 51 (10-11), 967–986.

Calambokidis, John, Steiger, Gretchen H., Curtice, Corrie, Harrison, Jolie, Ferguson, Megan C., Becker, Elizabeth, DeAngelis, Monica, Van Parijs, Sofie M., 2015. Biologically important areas for selected cetaceans within U.S. waters - west coast region. Aquat. Mamm. 41 (1), 39–53. https://doi.org/10.1578/AM.41.1.2015.39.

Carson, B., Baldauf, J.G., Westbrook, G.K., 1992. ODP Expedition: 146—Site: 893—Hole: A. http://web.iodp.tamu.edu/OVERVIEW/?&exp=146&site=893.

Checkley, David M., Barth, John A., 2009. Patterns and processes in the California current system. Prog. Oceanogr. 83 (1–4), 49–64. https://doi.org/10.1016/j.pocean.2009.07.028.

Chen, Chen-Tung, Millero, Frank J., 1977. Speed of sound in seawater at high pressures. J. Acoust. Soc. Am. 62 (5), 1129–1135. https://doi.org/10.1121/1.381646.

Chion, Clément, Lagrois, Dominic, Dupras, Jérôme, 2019. A Meta-analysis to understand the variability in reported source levels of noise radiated by ships from opportunistic studies. Front. Mar. Sci. Front. Media S.A. https://doi.org/10.3389/fmars.2019.00714.

Chou, Emily, Southall, Brandon L., Robards, Martin, Rosenbaum, Howard C., 2021. International policy, recommendations, actions and mitigation efforts of anthropogenic underwater noise. Ocean Coast. Manag. 202 (March) https://doi.org/10.1016/j.ocecoaman.2020.105427.

Collins, Michael D., 2001. User's Guide for RAM Versions 1.0 and 1.0p, p. 14.

Erbe, Christine, Schoeman, Renee P., Peel, David, Smith, Joshua N., 2021. It often howls more than it chugs: wind versus ship noise under water in Australia's maritime regions. J. Mar. Sci. Eng. 9 (5) https://doi.org/10.3390/jmse9050472.

Farcas, Adrian, Powell, Claire F., Brookes, Kate L., Merchant, Nathan D., 2020. Validated shipping noise maps of the Northeast Atlantic. Sci. Total Environ. 735 (September) https://doi.org/10.1016/j.scitotenv.2020.139509.

Gassmann, Martin, Wiggins, Sean M., Hildebrand, John A., 2017. Deep-water measurements of container ship radiated noise signatures and directionality. J. Acoust. Soc. Am. 142 (3), 1563–1574.

GEBCO Compilation Group, 2023. GEBCO 2023 Grid. https://doi.org/10.5285/f98b053b-0cbc-6c23-e053-6c86abc0af7b.

Hildebrand, John A., 2009. Anthropogenic and natural sources of ambient noise in the ocean. Mar. Ecol. Prog. Ser. 395, 5–20. https://doi.org/10.3354/meps08353.

Hildebrand, John A., Frasier, Kaitlin E., Baumann-Pickering, Simone, Wiggins, Sean M., 2021. An empirical model for wind-generated ocean noise. J. Acoust. Soc. Am. 149 (6), 4516–4533. https://doi.org/10.1121/10.0005430.

Levesque, Peter. 2011. The Shipping Point: The Rise of China and the Future of Retail Supply Chain Management. (page 30–50). John Wiley & Sons.

Macgillivray, Alexander, de Jong, Christ, 2021. A reference Spectrum model for estimating source levels of marine shipping based on automated identification system data. J. Mar. Sci. Eng. 9 (4) https://doi.org/10.3390/jmse9040369.

MacGillivray, Alexander O., Li, Zizheng, Hannay, David E., Trounce, Krista B., Robinson, Orla M., 2019. Slowing deep-sea commercial vessels reduces underwater radiated noise. J. Acoust. Soc. Am. 146 (1), 340–351. https://doi.org/10.1121/1.5116140.

Mackenzie, Kenneth V., 1981. Nine-term equation for sound speed in the oceans. J. Acoust. Soc. Am. 70 (3), 807–812. https://doi.org/10.1121/1.386920.

McDonald, Mark A., Hildebrand, John A., Wiggins, Sean M., 2006. Increases in deep ocean ambient noise in the northeast pacific west of San Nicolas Island, California. J. Acoust. Soc. Am. 120 (2), 711–718. https://doi.org/10.1121/1.2216565.

Mckenna, Megan F., Soldevilla, Melissa, Oleson, Erin, Wiggins, Sean, Hildebrand, John A., 2009. Increased Underwater Noise Levels in the Santa Barbara Channel from Commercial Ship Traffic and the Potential Impact on Blue Whales (*Balaenoptera musculus*). http://www.coaa.co.uk/.

McKenna, Megan F., Wiggins, Sean M., Hildebrand, John A., 2013. Relationship between container ship underwater noise levels and ship design, operational and oceanographic conditions. Sci. Rep. 3 https://doi.org/10.1038/srep01760.

Oleson, Erin M., Calambokidis, John, Burgess, William C., McDonald, Mark A., LeDuc, Carrie A., Hildebrand, John A., 2007. Behavioral context of call production by eastern North Pacific blue whales. Mar. Ecol. Prog. Ser. 330, 269–284. https://doi.org/10.3354/meps330269.

Redfern, Jessica V., Hatch, Leila T., Caldow, Chris, DeAngelis, Monica L., Gedamke, Jason, Hastings, Sean, Henderson, Laurel, McKenna, Megan F., Moore, Thomas J., Porter, Michael B., 2017. Assessing the risk of chronic shipping noise to baleen whales off Southern California, USA. Endanger. Species Res. 32 (1), 153–167. https://doi.org/10.3354/esr00797.

Ricciardulli, Lucrezia, and National Center for Atmospheric Research Staff. 2022. "The Climate Data Guide: CCMP: Cross-Calibrated Multi-Platform Wind Vector Analysis." 2022. https://climatedataguide.ucar.edu/climate-data/ccmp-cross-calibrated-multi-platform-wind-vector-analysis.

Ross, Donald, 1976. Mechanics of Underwater Noise. Pergamon Press, Pasadena, California.

Sertlek, Hüseyin Özkan, Slabbekoorn, Hans, ten Cate, Carel, Ainslie, Michael A., 2019. Source specific sound mapping: spatial, temporal and spectral distribution of sound in the Dutch North Sea. Environ. Pollut. 247, 1143–1157. https://doi.org/10.1016/j.envpol.2019.01.119.

Simard, Yvan, Roy, Nathalie, Gervaise, Cédric, Giard, Samuel, 2016. Analysis and modeling of 255 source levels of Merchant ships from an acoustic observatory along St. Lawrence seaway. J. Acoust. Soc. Am. 140 (3), 2002–2018. https://doi.org/10.1121/1.4962557.

Straume, E.O., Gaina, C., Medvedev, S., Hochmuth, K., Gohl, K., Whittaker, J.M., Abdul Fattah, R., Doornenbal, J.C., Hopper, J.R., 2019. GlobSed: updated Total sediment thickness in the World's oceans. Geochem. Geophys. Geosyst. 20 (4), 1756–1772. https://doi.org/10.1029/2018GC008115.

Szesciorka, Angela R., Ballance, Lisa T., Širović, Ana, Rice, Ally, Ohman, Mark D., Hildebrand, John A., Franks, Peter J.S., 2020. Timing is everything: drivers of interannual variability in blue whale migration. Sci. Rep. 10 (1), 7710.

United Nations. 2022. "United Nations *Conference on Trade and Development (UNCTAD): Navigating Stormy Waters*." 2022. New York.

Wang, Lian, Heaney, Kevin D., Pangerc, T., Theobald, P.D., Robinson, Stephen P., Ainslie, Michael A., 2014. Review of underwater acoustic propagation models. National Physical Laboratory 171 (6), 727–735. https://eje.bioscientifica.com/view/journals/eje/171/6/727.xml.

Wenz, Gordon M., 1962. Acoustic ambient noise in the ocean: spectra and sources. J. Acoust. Soc. Am. 34 (12), 1936–1956. https://doi.org/10.1121/1.1909155.

Wiggins, Sean, John, M., Hildebrand, A., 2007. High-frequency Acoustic Recording Package (HARP) for broad-band, long-term marine mammal monitoring. In: 2007 Symposium on Underwater Technology and Workshop on Scientific Use of Submarine cables and Related Technologies. IEEE, pp. 551–557.

ZoBell, Vanessa M., Frasier, Kaitlin E., Morten, Jessica A., Hastings, Sean P., Peavey, Lindsey E., Reeves, Sean M. Wiggins, Hildebrand, John A., 2021. Underwater noise mitigation in the Santa Barbara Channel through incentive-based vessel speed reduction. Sci. Rep. 11 (1), 18391.

ZoBell, Vanessa M., Gassmann, Martin, Kindberg, Lee B., Wiggins, Sean M., Hildebrand, John A., Frasier, Kaitlin E., 2023. Retrofit-induced changes in the radiated noise and monopole source levels of container ships. PLoS One 18 (3), e0282677.